

A system for high-speed microinjection of adherent cells

Wenhui Wang,^{1,a)} Yu Sun,^{2,b)} Ming Zhang,³ Robin Anderson,⁴ Lowell Langille,³ and Warren Chan⁴

¹Department of Mechanical Engineering, University of Canterbury, Private Bag 4800, Christchurch 8140, New Zealand

²Advanced Micro and Nanosystems Laboratory, University of Toronto, 5 King's College Road, Toronto, Ontario M5S 3G8, Canada

³Division of Cellular and Molecular Biology, Toronto General Research Institute, 101 College Street, Toronto, Ontario M5G 1L7, Canada

⁴Institute of Biomaterials and Biomedical Engineering, University of Toronto, 164 College Street, Toronto, Ontario M5S 3G9, Canada

(Received 7 August 2008; accepted 2 October 2008; published online 31 October 2008)

This paper reports on a semi-automated microrobotic system for adherent cell injection. Different from embryos/oocytes that have a spherical shape and regular morphology, adherent cells are flat with a thickness of a few micrometers and are highly irregular in morphology. Based on computer vision microscopy and motion control, the system coordinately controls a three-degrees-of-freedom microrobot and a precision XY stage, demonstrating an injection speed of 25 endothelial cells per minute with a survival rate of 95.7% and a success rate of 82.4% ($n=1012$). The system has a high degree of performance consistency. It is operator skill independent and immune from human fatigue, only requiring a human operator to select injection destinations through computer mouse clicking as the only operator intervention. The microrobotic system makes the injection of a large number of adherent cells practical for testing cellular responses to foreign molecules. © 2008 American Institute of Physics. [DOI: 10.1063/1.3006000]

I. INTRODUCTION

The injection of biological cells permits the insertion of foreign materials into individual cells for quantifying cellular responses and imaging intracellular structures.^{1–4} As an example application, *in vitro* investigation of intracellular behavior of nanoparticles [e.g., interactions between organelles and CdSe quantum dots (QDs)] has important implications in nanotoxicity, intracellular imaging, drug delivery, therapeutics, and the design of multifunctional nanoparticles.^{5–7} For testing five common types of coatings (bifunctionalized ligand, silanization, hydrophobic interaction, amphiphilic polymer, and hydroxylated⁸) to target six potential organelle candidates including mitochondria, centrosome, golgi, lysosome, vacuole, and ribosome, each combination would require the injection of a minimum of 1000 mammalian cells to obtain statistically significant data, amounting to a total of 30 000 cells. The enormous number of cells to be injected makes the manual operation impractical, calling for a high-speed injection system.⁹

In robotics research, efforts for automating cell injection have been continuous. The vast majority of these systems^{10–16} were developed to facilitate the handling of mouse/*Drosophila*/zebrafish embryos/oocytes for genetics and reproduction applications. In microrobotic injection of suspended cells (e.g., embryos/oocytes), cells must be immobilized, preferably into a regular pattern to minimize cell searching and switching tasks and increase injection speed.¹⁶

Differently, most mammalian cells (e.g., HeLa cells, fibroblasts, and endothelial cells) adhere to the bottom surface of a culture dish/plate during *in vitro* culture.¹⁷ Although adherent cells do not require immobilization efforts, they are highly irregular in morphology (Fig. 1), which makes robust pattern recognition difficult and full automation challenging. Additionally, they are only a few micrometers thick, posing more stringent requirements in microrobotic positioning.

Compared to microinjection of suspended cells, fewer robotic systems were developed for the injection of adherent cells.^{18–21} Existing systems are either manually operated via joysticks,^{18–20} which is labor intensive and causes performance inconsistencies, or involve complex, delicate hardware^{21,22} that is employed to determine the vertical position of the micropipette with respect to target cells. Besides

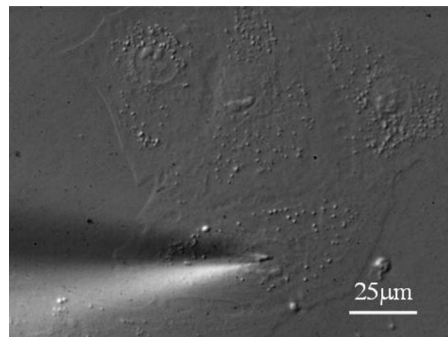


FIG. 1. Injection of endothelial cells that are 3.8–5.5 μm thick with nucleus higher than cytoplasm. Nucleus (e.g., the circular shape under the micropipette tip) is around 15 μm in diameter.

^{a)}Electronic mail: wenhui.wang@canterbury.ac.nz.

^{b)}Electronic mail: sun@mie.utoronto.ca.

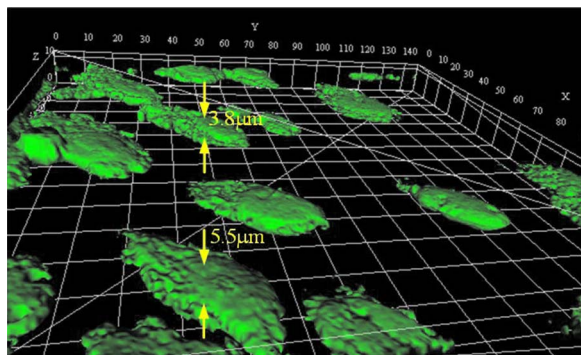


FIG. 2. (Color online) 3D profile of endothelial cells. Reconstructed from a stack of confocal fluorescence images.

adding additional costs, the complex and delicate hardware requires precisely controlled working conditions, increasing operation complexity, and reducing system reliability.

As one type of mammalian adherent cells, endothelial cells were chosen for demonstration in this paper. Endothelial cells line the entire circulatory system from the heart to the smallest capillary, playing important roles in the vascular system. Figure 2 shows a three-dimensional (3D) profile of endothelial cells reconstructed from a stack of confocal fluorescence images. Cells cultured at the bottom of a Petri dish are flat with a thickness varying from 3.8 to 5.5 μm , with nucleus as the protruding part.

The small thickness and large variations require accurate determination of the relative vertical positions between the injection micropipette and a cell. A reported method employed electrodes inside the injection micropipette and culture dish²² to detect the contact between the micropipette and a cell. Detection was conducted through monitoring impedance changes. Factors that could induce detection errors are the type and concentration of cell media and injection solutions.

The system presented in this paper operates semi-automatically, requiring a human operator to select injection destinations through computer mouse clicking as the only operator intervention. Based on computer vision microscopy, our contact detection approach is capable of detecting micropipette-Petri dish contact without requiring additional force/touch or impedance sensors,²³ demonstrating an accuracy of 0.2 μm with high robustness and repeatability with respect to illumination, motion speed, and microscopy magnification.

II. SYSTEM DESIGN

A. System setup

The system, shown in Fig. 3, employs a three-degrees-of-freedom microrobot (MP-285, Sutter) with a travel of 25 mm and a 0.04 μm positioning resolution along each axis. One motion control card (NI PCI-6289) is mounted on a host computer (3.0 GHz CPU, 1Gbyte memory) where control algorithms operate. Visual feedback is obtained through a complementary metal-oxide-semiconductor camera (A601f, Basler) mounted on an inverted microscope (IX81, Olympus). A polystyrene Petri dish (55 mm, Falcon), where en-

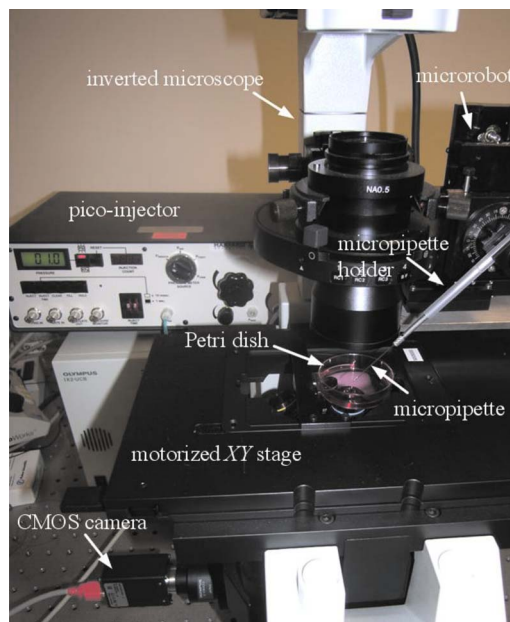


FIG. 3. (Color online) Microrobotic system for adherent cell injection.

dothelial cells are seeded, is placed on a motorized precision XY stage (ProScanII, Prior). A glass micropipette, heated and pulled using a micropipette puller (P-97, Sutter), is connected to the microrobot via a micropipette holder. The micropipette is tilted 45° with respect to the XY stage. A computer-controlled pico-injector (PLI-100, Harvard Apparatus) with a femtoliter resolution provides positive pressure for material deposition. All units except the host computer and pressure unit are placed on a vibration isolation table. The coordinate frames of the system defined in Fig. 4 are summarized in Table I.

Ideally, all the axes should be identical to the directions shown in Fig. 4. However, the assembly of the whole system cannot be perfect in reality, causing each axis to deviate with several degrees. This systematic error could be measured and easily compensated for a specific experiment assembly.

B. Micropipette processing

Injection of mammalian adherent cells requires the use of injection micropipettes with a tip of 0.1–1 μm in the outer diameter (OD) in order to minimize cell damage and to warrant a high survival rate. Many micropipette processing parameter combinations were tested. Scanning electron microscopy (SEM) was used to accurately measure the inner diameter (ID) and OD of pulled micropipettes. Table II summarizes the selected sets of processing parameters and the resulting micropipette tip sizes.

With a tip of OD/ID=0.54/0.27 μm or smaller, QDs rapidly aggregated at the tip end and caused clogging. In this study, micropipette tips with an OD/ID of 0.87/0.6 μm were selected since clogging was greatly suppressed and cell damage was insignificant. Figure 5 shows a SEM image of a micropipette tip with OD/ID of 0.87/0.6 μm .

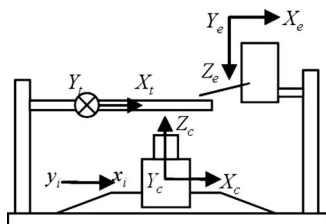


FIG. 4. Coordinate frames of the system.

C. Injection volume control

The volume of foreign materials inserted into a cell should not exceed 5% of the cell's cytoplasmic volume. Volume calibration is also critical for precisely depositing a specified amount of materials into individual cells such that dose effects can be investigated. The pico-injector used in this work provides a calibrated formula relating the injection volume to the applied pressure, pressure "on" time (i.e., pulse length), and the tip inner diameter. By controlling the pressure level and pressure pulse length, ~ 2 fl material was deposited into each endothelial cell (in either nucleus or cytoplasm) in the experiments with a high reproducibility.

III. CONTACT DETECTION

In order to deposit materials within a cell (Fig. 6), the relative vertical positions of the micropipette tip and the Petri dish surface along the Z_e direction must be accurately known before injection starts. As operation speed and robustness are prioritized, low complexity in system setup is highly desirable. Without the inclusion of an extra sensor (e.g., touch or force sensor), a computer vision-based contact detection technique²³ was developed for accurately determining the relative heights of the micropipette tip (controlled by the microrobot) and the surface of the Petri dish where cells are seeded.

For contact detection, the micropipette first moves only along the Y_e direction to identify the micropipette tip. Upon identification, the x - and y -coordinates in the image plane i and the X_e - and Y_e -coordinates of the micropipette tip at the end-effector frame e are determined and used to establish the transformation between the image frame and the X_e - Y_e plane.

After the identification of the micropipette tip, the micropipette moves only along the vertical direction (Z_e) to establish contact with the surface. After the establishment of contact in the world frame, further vertical motion of the micropipette tip induces horizontal motion in the image plane. Before and after contact, the x -coordinates of the mi-

TABLE II. Pulled micropipette tip size under various puller settings. (Micropipette pulling parameters. Ramp value: 479. Starting glass tubing: OD/ID=1.0/0.78 μm .)

Heat	Pull	Velocity	Time	Pressure	OD/ID (μm)
500	60	60	250	300	0.54/0.27
500	58	60	250	300	0.67/0.35
500	60	50	250	300	0.68/0.35
500	55	60	250	300	0.73/0.4
500	58	50	250	300	0.87/0.6
500	55	50	250	300	1.28/0.9
500	50	50	250	300	1.69/1.21

cropipette tip in the image plane i result in a V-shaped curve. Searching for the global minimum locates the peak of the curve that represents the contact position. The entire contact detection process is completed between 6 and 10 s, achieving an accuracy of 0.2 μm . Under a high magnification of 40 \times , the microrobot vertical speed was controlled not to exceed 1 $\mu\text{m/s}$ in order to avoid micropipette breakage, which is limited by the speed of image processing.

Although phase contrast or differential interference contrast (DIC) produces desired visualization effects (pseudo-3D view of cells) for cell imaging [Fig. 7(a)], due to the small micropipette tip size, it was found in experiments that the bright-field imaging mode is more favorable for contact detection. Under bright field, the tip pattern is more uniform and "halo" free [Fig. 7(b)], resulting in a more reliable tracking and better reproducibility in contact detection. Note that bright field is used only for contact detection. Imaging is switched to phase contrast or DIC for the rest of the injection procedures.

With the initial contact between the micropipette tip and the Petri dish surface accurately determined, the microrobot moves upward by 8 μm above the contact position, which is slightly greater than the cell height (~ 5 μm) to prevent possible crashing with a cell when switching from one cell to the next. The Z_e -coordinate of injection destinations for material deposition was set at 3 μm above the contact position.

For a submicrometer-sized micropipette tip, clogging due to cell debris accumulation and impurity of injection materials is unavoidable. Micropipette tips with OD/ID of 0.87/0.6 μm used in the experiments typically became

TABLE I. Summary of coordinate frames.

Symbol	Coordinate frame
e	End-effector coordinate frame X_e - Y_e - Z_e attached to microrobot that controls the motion of the injection micropipette
t	Target coordinate frame X_t - Y_t - Z_t attached to motorized XY stage that controls the motion of cells
c	Camera coordinate frame X_c - Y_c - Z_c
i	Image plane x_i - y_i (or x - y)

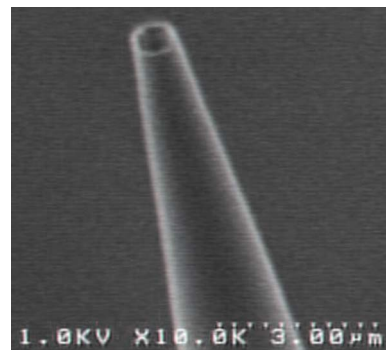


FIG. 5. (Color online) SEM image of a pulled tip with OD/ID = 0.87/0.6 μm .

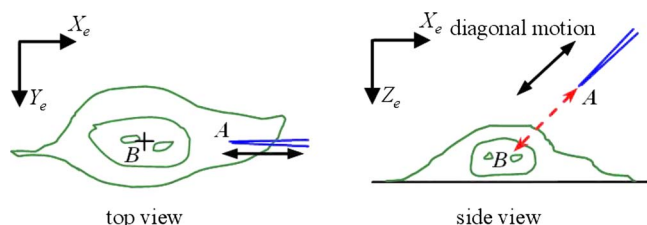


FIG. 6. (Color online) The injection micropipette tip moves along the diagonal direction from its initial position A to the selected destination B for material deposition. A and B are chosen to be 8 and 3 μm above the Petri dish surface.

clogged after injecting 50 endothelial cells. Every micropipette exchange requires the redetermination of relative vertical positions of the micropipette tip and Petri dish surface, which is greatly facilitated by the automated contact detection technique.

IV. MICROROBOTIC ADHERENT CELL INJECTION

A. Overall sequence

A Petri dish with cells seeded is placed on the motorized XY stage. Injection starts with vision-based contact detection to automatically determine the vertical positions of the micropipette tip and the surface of the Petri dish (Fig. 8). For all cells within the field of view, a human operator selects deposition destinations by computer mouse clicking in the control program interface. Based on the operator input coordinates in the image plane, the system determines the shortest injection path, according to which the micropipette tip moves to a cell, penetrates the cell membrane, deposits the specified volume of materials, retracts out of the cell, moves upward by 8 μm above the contact position, and then switches to the next cell for injection.

After all cells within the field of view are injected, the precision XY stage positions the Petri dish to bring the next segment of cells into the field of view. The injection process is repeated until all cells in the desired segments of the Petri dish are injected. During system operation, although the Petri dish is two-dimensional positioned by the XY stage, the microrobot is served along the three axes. Proportional-integral-derivative (PID) control is employed for positioning both the microrobot and the XY stage.

B. Injection path optimization

The system presently operates on the basis of mouse clicking in a batch mode plus shortest path calculation. In a random order, the human operator selects the x - and y -coordinates in the image plane as injection destinations for all cells within the field of view. The system employs the classical traveling salesman algorithm²⁴ to generate the shortest path (Fig. 9), which costs ~ 0.1 s for computation as

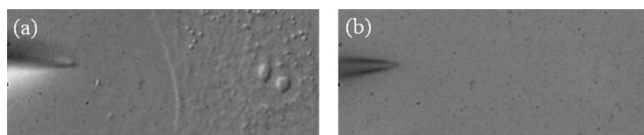


FIG. 7. (a) Under phase contrast (40 \times). (b) Under bright field (40 \times).

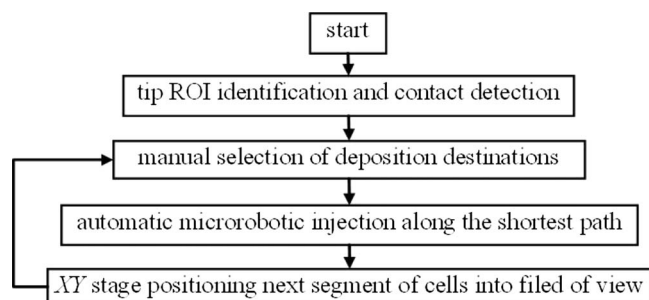


FIG. 8. Control flow of semi-automated microrobotic adherent cell injection.

each field of view contains only approximately ten cells. The injection sequence can either be clockwise or counterclockwise.

The above injection path optimization is conducted upon the determination of all destinations. It is particularly preferable for future integration of pattern recognition of cells, which provides deposition destinations without requiring human input. For the current semi-automated system, an alternative injection mode might be one click and one injection: once a destination is determined, the injection is performed. This single cycle repeats for all cells. This parallel mode allows for an operator to select next destination while the injection is ongoing, with potential to increase the throughput. Nevertheless, it does not work after pattern recognition is integrated into the system, as human input is not required any more.

C. Microrobotic control

Motion control of the microrobot is based on position feedback of the microrobot (Fig. 10) according to the PID control law. The microrobot and the PID controller are capable of producing a positioning accuracy better than 0.1 μm along all three axes. The transformation between the x - and y -coordinates in the image plane i and the X_e - and Y_e -coordinates of the micropipette tip in the end-effector frame e is established during contact detection (Sec. III) without requiring an off-line process. From operator input image coordinates, the lateral components of target position P_d for the micropipette tip are thus determined for each cell. Based on the confocal microscopy measured heights of endothelial cells, the vertical component of target position P_d was set at 3 μm above the contact position (i.e., Petri dish bottom surface) for all cells. The micropipette penetrates the

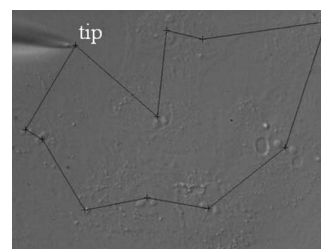


FIG. 9. Injection path. “+” represents a user selected injection destination. The system generates the shortest path.

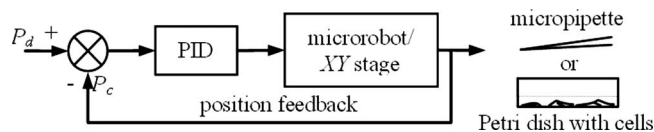


FIG. 10. Motion control of the microrobot and XY stage is based on PID position control.

membrane of a cell and retracts out of the cell both along the diagonal direction, as shown in Fig. 6.

D. XY stage position control

Under $40\times$ magnification, the number of cells in one field of view is limited (approximately ten). The Petri dish's bottom surface is "virtually" divided into many adjacent rectangular segments, with each segment corresponding to one field of view in the image. Microinjection is conducted from segment to segment. The target position P_d in the X_t - Y_t plane for the XY stage (Fig. 10) corresponds to the physical size of a segment, which is determined by the image size and calibrated pixel sizes (the calibrated pixel sizes are $0.255 \times 0.24 \mu\text{m}^2$ in our system).

V. EXPERIMENTAL RESULTS AND DISCUSSION

A. Materials

The cells used in the experiments were primary porcine aortic endothelial cells, isolated from porcine aorta and cultured in cell medium (M199 medium, 5% calf serum, and 5% fetal bovine serum with a pH value of 7.4). Microrobotic injection was performed after 2 or 3 days of cell passage.

During system testing, both fluorescent dyes (dextran, Texas Red, 70 000 molecular weight, neutral, Invitrogen) mixed with phosphate buffered saline buffer and CdSe/ZnS QDs coated with 40% octadecylamine modified poly(acrylic acid) (wavelength=586 nm) with a concentration of $1 \mu\text{M}$ were injected. The size of QDs with coating is $17.2 \pm 1.2 \text{ nm}$.

B. Results and discussion

The semi-automated microrobotic system injected a total of 1012 endothelial cells, demonstrating an operation speed of 25 cells/min. Cytoplasm instead of nucleus was selected as the injection destination for each cell. The injected cells were inspected under a fluorescence microscope (IX81, Olympus), excited by 540 nm laser light, and observed through a tetramethyl rhodamine isothiocyanate filter set. Visual inspection was conducted right after injection. Figure 11 shows microrobotically injected endothelial cells under both bright-field [Fig. 11(a)] and fluorescence microscopy [Fig. 11(b)]. The deposited fluorescent dyes (high brightness) can be clearly observed in the cells. Normal cell morphology is maintained after injection.

To quantitatively evaluate the performance of the microrobotic adherent cell injection system, two measures were defined. (1) *Survival rate*: this measure is defined as the ratio between the number of live cells after injection and the total number of cells injected, essentially representing the severity and frequency of cell damage from injection. Based on the

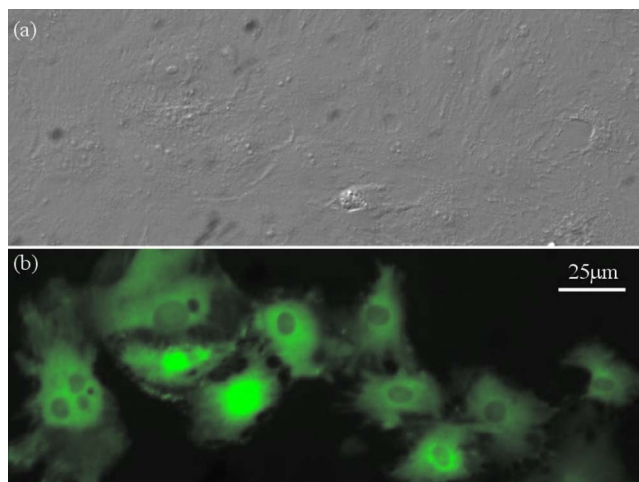


FIG. 11. (Color online) Cells injected with fluorescent dyes. (a) Bright-field image showing normal cell morphology is maintained after injection. (b) Fluorescence microscopy image.

1012 injected endothelial cells, the microrobotic injection system produced a survival rate of 95.7%, which was determined through Trypan blue exclusion testing of cell viability. (2) *Success rate*: this measure is defined as the ratio between the number of cells with materials successfully deposited inside the cell and the total number of injected cells. Essentially, this measure represents the reliability and the reproducibility of the system. Visual inspection revealed that the success rate of the 1012 injected endothelial cells was 82.4%.

The semi-automated microrobotic system achieving an operation speed of 25 adherent cells/min, a survival rate of 95.7%, and a success rate of 82.4% compares favorably with the manual injection (statistics from two highly skilled injection technicians at the University of Toronto: 5 cells/min, 80% survival rate, and 40% success rate). Additionally, the system is immune from large variations in performance since efforts from operator intervention are trivial (computer mouse clicking) without causing human fatigue as in manual injection. The system has a high degree of performance consistency, independent of proficiency differences across operators, although skilled operators can finish recognizing cells and selecting the injection destinations more quickly than unskilled operators.

The 82.4% success rate implies that 17.6% of the injection operation failed to deposit materials into a cell, mostly due to the following reasons: (1) the height/thickness variation across cells is significant. The vertical injection position of the micropipette tip was set at $3 \mu\text{m}$ above the Petri dish surface for all cells. The lack of accurate knowledge on individual cell heights causes failure occasionally. This problem can be tackled by using confocal microscopy as the imaging platform, which will enable cell height measurements but slow down the microinjection speed. (2) In our study, commercial Petri dishes commonly used in a biology laboratory were used for cell culturing and microinjection. The surface flatness was found to often vary by $1\text{--}2 \mu\text{m}$ even within a small neighborhood. Variations in surface flatness (i.e., unevenness) can cause the micropipette tip to either fail

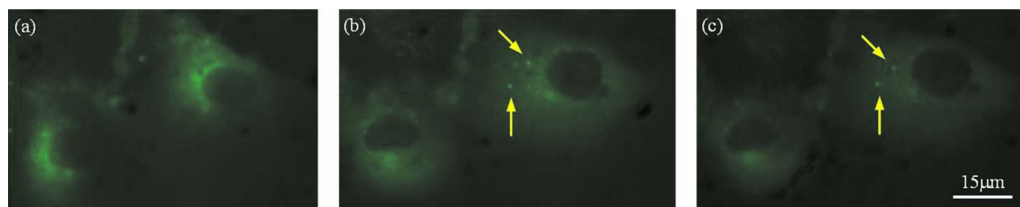


FIG. 12. (Color online) Cells injected with QDs: (a) right after injection, (b) 1 h after injection, and (c) 2 h after injection. The aggregated QDs are labeled by arrows.

to enter a cell or penetrate through a cell. The use of specially made substrates with more even flatness is expected to greatly alleviate this problem and further increase the success rate.

In the preliminary experiments of QD injection, the QD injected endothelial cells were cultured at 37 °C in a CO₂ incubator and visually inspected under fluorescence microscopy. Figure 12 shows the fluorescence images of two QD injected cells right after injection, 1 h after injection, and 2 h after injection. It appears that QDs gradually diffused throughout cytoplasm but without entering the nucleus. Some QDs seemed to form aggregates [arrow labeled in Figs. 12(b) and 12(c)] possibly around specific organelles. In order to determine if QDs with a particular coating truly aggregate around an organelle in a selective manner, it is required to selectively stain one organelle at a time and repeat the injection of QDs with different coatings into a large number of cells with the microrobotic adherent cell injection system. Thorough QD testing is part of our on-going research. Future work also includes the development of a robust image processing algorithm for recognizing highly irregular adherent cell structures, which will eliminate the need for a human operator to specify injection destinations in order to realize a fully autonomous system.

ACKNOWLEDGMENTS

Y. Sun acknowledges the funding agencies for supporting this project: the Natural Sciences and Engineering Research Council of Canada for awarding a Discovery Grant and the Ontario Ministry of Research and Innovation for awarding an Early Researcher Award.

¹K. H. Reuner, A. V. D. Does, P. Dunker, I. Just, K. Aktories, and N. Katz, *Biochem. J.* **319**, 843 (1996).

²A. Kalota, S. E. Shetzline, and A. Gewirtz, *Cancer Biol. Ther.* **3**, 4 (2004).

³A. M. Derfus, W. C. W. Chan, and S. N. Bhatia, *Adv. Mater. (Weinheim, Ger.)* **16**, 961 (2004).

⁴G. L. Beretta, P. Perego, and F. Zunino, *Curr. Med. Chem.* **13**, 3291 (2006).

⁵A. Hoshino, K. Fujioka, T. Oku, S. Nakamura, M. Suga, Y. Yamaguchi, K. Suzuki, M. Yasuhara, and K. Yamamoto, *Microbiol. Immunol.* **48**, 985 (2004).

⁶B. D. Chithrani, A. A. Ghazani, and W. C. W. Chan, *Nano Lett.* **6**, 662 (2006).

⁷N. Q. Jia, Q. Lian, H. B. Shen, C. Wang, X. Y. Li, and Z. N. Yang, *Nano Lett.* **7**, 2976 (2007).

⁸J. M. Klostranec and W. C. W. Chan, *Adv. Mater. (Weinheim, Ger.)* **18**, 1953 (2006).

⁹P. Scherp and K. H. Hasenstein, *Adv. Space Res.* **31**, 2221 (2003).

¹⁰Y. Sun and B. J. Nelson, *Int. J. Robot. Res.* **21**, 861 (2002).

¹¹R. Kumar, A. Kapoor, and R. H. Taylor, *IEEE International Conference on Intelligent Robots and Systems (IROS'2003)*, Las Vegas, 2003 (unpublished), p. 3186.

¹²K. Schnizler, M. Kster, C. Methfessel, and M. Fejt, *Recept. Channels* **9**, 41 (2003).

¹³S. Zappe, M. Fish, M. P. Scott, and O. Solgaard, *Lab Chip* **6**, 1012 (2006).

¹⁴A. Pillarisetti, M. Pekarev, A. D. Brooks, and J. P. Desai, *IEEE Trans. Autom. Sci. Eng.* **4**, 322 (2007).

¹⁵L. Mattos, E. Grant, R. Thresher, and K. Kluckman, *IEEE International Conference on Robotics and Automation (ICRA'2007)*, Rome, Italy, 2007 (unpublished), p. 1924.

¹⁶W. H. Wang, X. Y. Liu, D. Gelin, B. Ciruna, and Y. Sun, *PLoS ONE* **2**, e862 (2007).

¹⁷P. J. Reddig and R. L. Juliano, *Cancer Metastasis Rev.* **24**, 425 (2005).

¹⁸H. Matsuoka, Y. Yamada, K. Matsuoka, and M. Saito, *Biotechnology in Agriculture and Forestry* **58**, 339 (2006).

¹⁹H. Matsuoka, T. Komazaki, Y. Mukai, M. Shibusawa, H. Akane, A. Chaki, N. Uetake, and M. Saito, *J. Biotechnol.* **116**, 185 (2005).

²⁰K. Viigipuu and P. Kallio, *ATLA* **32**, 417 (2004).

²¹P. Kallio, T. Ritala, M. Lukkari, and S. Kuikka, *Int. J. Robot. Res.* **26**, 1303 (2007).

²²M. J. Lukkari, M. I. Karjalainen, R. Sarkanen, M.-L. Linne, T. O. Jalonen, and P. J. Kallio, *Proceedings of the 26th International Conference (IEEE) on Engineering in Medicine and Biology Society (EMBS'2004)*, San Francisco, 2004 (unpublished), p. 2557.

²³W. H. Wang, X. Y. Liu, and Y. Sun, *Int. J. Robot. Res.* **26**, 821 (2007).

²⁴D. L. Applegate, R. E. Bixby, V. Chvtal, and W. J. Cook, *The Traveling Salesman Problem: A Computational Study* (Princeton University Press, Princeton, NJ, 2006).